Advanced Journal of Chemistry, Section A

Journal homepage: www.ajchem-a.com

Original Research Article

Enhanced Trypan Blue Removal from Wastewater Using Surface-Modified MOF-5 Adsorbents

Hassan Aberrwaila[1,2], Hajer Chemingui[2,*], Amor Hafiane[2], Madiha Kamoun[2]

[1]*Chemistry Department, Faculty of Science, Al-Manar University, Tunisia, Tunisia*
[2]*Laboratory of Water, Membranes and Environmental Biotechnology, Water Researches and Technologies Center, BP 273, Soliman 8020, Tunisia*

ARTICLEINFO

Article history

Submitted: 2025-11-27
Revised: 2026-01-07
Accepted: 2026-02-15
ID: AJCA-2511-1983
DOI: 10.48309/AJCA.2026.562486.1983

KEYWORDS

Adsorption
MOF-5
Wastewater
Dye removal
Isotherm

ABSTRACT

The present study shows the synthesis of porous materials MOF-5 via a solvothermal method for wastewater treatment, particularly in the processes of capturing and removing Trypan blue (TB) dye from water. The structural and morphological properties of the synthesized MOF-5 were characterized using X-ray diffraction (XRD), Fourier-transform infrared spectroscopy (FT-IR), scanning electron microscopy (SEM), and thermogravimetric analysis (TGA). At optimized conditions (pH = 3, T = 25 °C), MOF-5 demonstrated a maximum TB removal efficiency of 77%. Adsorption isotherm studies indicated that the process was best described by the Langmuir model, suggesting monolayer adsorption with a calculated maximum adsorption capacity (Q_{max}) of 25 mg/g. Kinetic studies showed that the adsorption followed a pseudo-second-order model. Furthermore, thermodynamic parameters confirmed that the adsorption process was spontaneous and endothermic. These findings demonstrate that MOF-5 is a promising adsorbent for dye removal from wastewater, with potential for scaling up from laboratory to industrial applications.

GRAPHICAL ABSTRACT

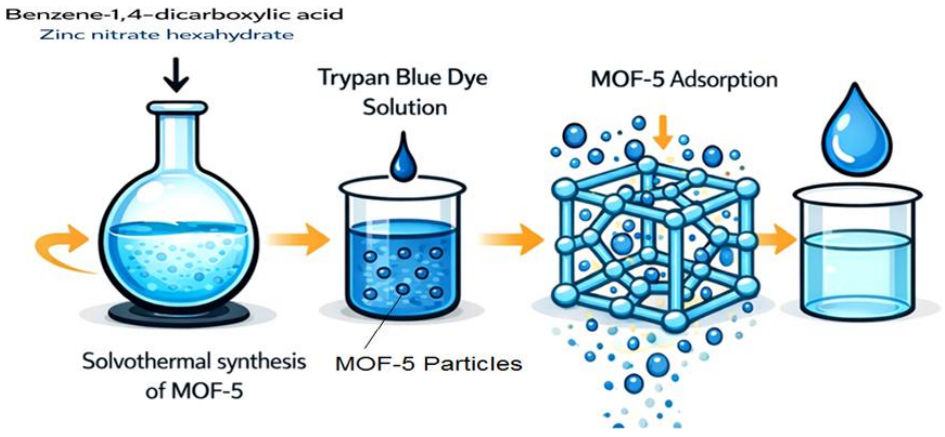

* Corresponding author: Chemingui, Hajer
✉ E-mail: hajerchemingui2@gmail.com

Introduction

The discharge of dye-containing industrial effluents into water bodies represents a significant environmental challenge due to its detrimental effects on human health and aquatic ecosystems [1,2]. Industrial expansion has led to the widespread application of synthetic dyes, which are recalcitrant (resistant to degradation) and often carcinogenic. Consequently, their discharge without adequate treatment presents a significant threat to environmental and human health [3,4]. The paper, textile, tanning, cosmetics, and pharmaceutical industries are among the major sources of water pollution caused by dyes [5]. The explosive growth of the textile industry in recent years has caused substantial dye discharge into water sources [6]. Trypan blue (TB) is one of the most commonly used dyes in various industrial, medical, and biological applications [7,8]. According to the International Agency for Research on Cancer (IARC), TB is classified as a carcinogen, making its removal essential to mitigate its adverse effects on human health and the environment [9]. A range of techniques can be employed to remove dyes from contaminated wastewater, including ozonation, photocatalysis, adsorption, oxidation, photolysis, biodegradation, and membrane separation [10-12], Although most of these technologies may encounter limitations regarding effectiveness and economic feasibility, adsorption has emerged as a highly promising and efficient approach for water purification [13]. A range of materials has been studied, including inorganic substances like magnesium oxide and zinc oxide nanoparticles, natural biomass such as ground avocado seeds, phosphate sludge used as a porogen in ceramic membrane fabrication, and polymers like polyvinyl alcohol (PVA) [14–18]. Additionally, various composite materials, such as Nitrogen-doped zeolite biochar (NZB), have been explored to enhance adsorption efficiency [19], while conventional adsorbents and composites have demonstrated varying degrees of efficiency in removing TB and other dyes. However, conventional materials often suffer from limitations such as high cost and low reusability, driving the search for more cost-effective alternatives [20,21]. Consequently, there is a significant need for alternative adsorbents that are high-capacity, low-cost, and sustainable. Recently, advanced porous materials, particularly metal–organic frameworks (MOFs), have been investigated for dye removal from wastewater owing to their unique properties, most notably their exceptionally high surface-to-volume ratio [22-24]. Among these, MOF-5 is highly promising due to its high surface area and porous structure. These properties make it suitable for applications ranging from drug delivery and gas storage to water treatment [25]. Its framework is composed of ZnO clusters primarily connected by tetra-coordinated 1,4 benzenedicarboxylate (BDC) linkers [26,27]. The efficiency of MOF-5 in the adsorption of heavy metals and dyes from aqueous solutions has been demonstrated in a number of experiments. For example, MOF-5 has shown an exceptionally high adsorption capacity for methyl orange (MO), surpassing many traditional adsorbents by a wide margin [28]. Similarly, MOF-5 and its composites, such as MOF-5/graphene oxide (MOF-5@GO), have demonstrated excellent performance in the removal of Rhodamine dye [29]. Furthermore, it has been reported that incorporating MOF-5 into hybrid systems enhances their stability and reusability [30,31]. This confirms the significant potential of MOF-5 in wastewater treatment applications. This study aimed to synthesize MOF-5 as a hybrid material for treating wastewater contaminated with TB dye. The synthesized material was characterized using scanning electron microscopy (SEM), Fourier-transform infrared spectroscopy (FTIR), X-ray diffraction (XRD), and thermogravimetric analysis (TGA). The effectiveness of this adsorbent for TB removal was evaluated under specific experimental

conditions. Additionally, the adsorption behavior was comprehensively evaluated through thermodynamic and kinetic modeling. This work demonstrates the untapped potential of MOF-5 for the removal of complex anionic dyes, such as TB dye, from aqueous solutions using a simple synthesis method involving a Teflon-lined stainless-steel autoclave. In contrast to previous studies that primarily focused on MOF-5 for other applications, including gas storage and the adsorption of colorless organic compounds. The novelty of this study lies in its detailed thermodynamic evaluation and the optimization of operational conditions pH, adsorbent amount, starting concentration, and contact time to achieve high removal efficiencies, both of which have been rarely explored in MOF-5-based systems. This study aimed to synthesize MOF-5 via a solvothermal method and to evaluate its efficacy as an adsorbent for the removal of TB dye from aqueous solutions. The main objectives are defined by three primary goals that distinguish it from prior research: i) to investigate the novel application of MOF-5 for the adsorption of TB dye, representing the first comprehensive study of this specific adsorbent-adsorbate pair; ii) to provide a complete mechanistic analysis through detailed optimization of operational parameters and systematic modeling of adsorption isotherms, kinetics, and thermodynamics and iii) to rigorously assess the practical potential and economic feasibility of MOF-5 by evaluating its stability and reusability across multiple adsorption-desorption cycles. This work uniquely integrates a novel target pollutant with a thorough process analysis and a direct investigation of regenerative performance, offering new insights for advancing MOF-based technologies in practical wastewater treatment. The raw materials used were benzene-1,4-dicarboxylic acid (H2BDC), zinc nitrate hexahydrate ($Zn(NO_3)_2{\cdot}6H_2O$), and *N*,*N*-dimethylformamide (DMF). Overall, this work offers meaningful insights into the effectiveness of hybrid materials in wastewater treatment.

Methodology

Experimental materials and methods

TB dye ($C_{34}H_{28}N_6O_{14}S_4$) was purchased from Merck, Germany, with a purity of 99.9%. It was obtained in powder form, with a molecular weight of 960 g/mol, for the preparation of all solutions. Zinc nitrate hexahydrate [$Zn(NO_3)_2{\cdot}6H_2O$] was purchased from Daejung (>99%, China). Benzene-1,4-dicarboxylic acid (H_2BDC, 98%) and DMF (extra pure, 99%) were supplied by Sisco Research Laboratories Pvt. Ltd., India. Sodium hydroxide (NaOH, 0.1 M) and hydrochloric acid (HCl, 0.1 M) were obtained from Sigma-Aldrich (98%, Germany). All chemicals and reagents were used as received without further purification.

Preparation of MOF-5

Figure 1 illustrates the steps involved in the melt synthesis of MOF-5 using a Teflon-lined stainless-steel autoclave, with slight modifications to a previously reported procedure [32]. Briefly, 3.86 g of zinc nitrate hexahydrate (0.7 M) was dissolved in 40 mL of DMF under magnetic stirring until a clear solution was obtained. Separately, 0.82 g of benzene-1,4-dicarboxylic acid (0.2 M) was dissolved in another 40 mL of DMF under identical conditions. The two prepared solutions were mixed and stirred at 50 °C for 40 min. The mixture was then placed into a 100 mL Teflon-lined stainless-steel autoclave and treated solvothermally at 130 °C for 22 h. After cooling to room temperature, the resulting white crystals were separated by centrifugation at 4,000 rpm for 10 min, rinsed three times with DMF, and dried at 60 °C for 24 h.

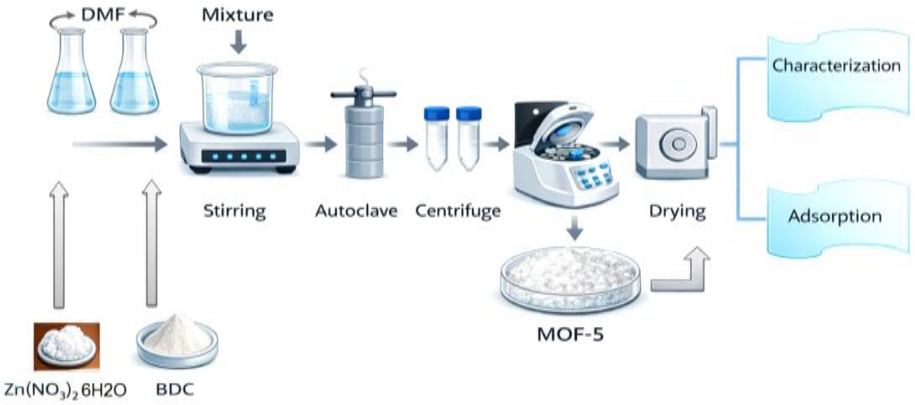

Figure 1. Synthesis of MOF-5

Characterization techniques

A set of analytical techniques was used to confirm the successful preparation of the sorbent. The crystalline structure of MOF-5 was characterized using XRD (D8 ADVANCE, Bruker, Germany). FTIR (PerkinElmer FTIR 2000, Germany) was performed in the 4000–400 cm^{-1} range using KBr pellets to determine the functional groups in the samples. The surface morphology and structural features of the synthesized material were observed using a scanning electron microscope (FEI Q250/EDAX, Thermo Fisher, Germany). Additionally, thermogravimetric analysis (TGA, TA Q500, USA) was conducted to assess the thermal stability of the produced material [32].

Adsorption study

A series of adsorption experiments was conducted under various controlled conditions, including pH (2–12), initial TB concentrations (10–120 ppm), adsorbent dosages (0.01–0.4 g/L), and contact times (10–240 min). The pH was adjusted using 0.1 M HCl and 0.1 M NaOH. Adsorption tests were performed at room temperature (25 ± 3 °C) with continuous stirring (170 rpm) for 2 h. After centrifugation at 4000 rpm for 15 min. The remaining dye concentration was determined using a UV–Vis spectrophotometer (SHIMADZU UV-1900, Japan) at a wavelength of 607 nm. The removal efficiency and adsorption capacity were then calculated according to the corresponding Equations 1 and 2:

$$q_e = \frac{C_0 - C_e}{M} \times V \quad (1)$$

$$TB\ \% = \frac{C_0 - C_e}{C_0} \times 100 \quad (2)$$

Where, q_e represents the adsorption capacity of the adsorbent (mg/g), C_0 and C_e are the initial and final concentrations of TB dye (ppm), respectively, M is the adsorbent weight (g), and V is the volume (mL) of TB dye solution. To determine the point of zero charge (pH_{pzc}), 50 mg of MOF-5 was equilibrated for 48 hours with 50 mL of 0.5 M NaCl solutions whose initial pH had been adjusted across a range of 1 to 12 [33]. The pH_{pzc} was subsequently determined from a plot of the final pH against the initial pH, defined as the point where the two values were equal.

Isotherm modeling

Adsorption isotherm models are commonly employed to describe adsorption behavior and to estimate key parameters, such as the maximum adsorption capacity (Q_{max}) and the correlation coefficient (R^2). These models also provide insights into the adsorption mechanism and the distribution of adsorbates between the liquid and solid phases. In this study, three isotherm models

were applied to evaluate the adsorption of TB dye onto MOF-5: Langmuir, Freundlich, and Temkin; each isotherm model provides specific insights into the adsorption mechanism. The Langmuir model assumes monolayer adsorption on a homogeneous adsorbent surface with a finite number of identical and energetically equivalent sites [34]. Its linear form is expressed as follows:

$$\frac{C_e}{qe} = \frac{C_e}{Qmax + \frac{1}{Qmax}.b} \quad (3)$$

Where, C_e is the initial concentration (ppm), q_e refers to the adsorption capacity at equilibrium, Q_{max} indicates the maximum adsorption capacity, and b is the Langmuir parameter expressed in L/mg. The separation factor or equilibrium parameter, R_L, is commonly used to predict the favorability of an adsorption process in the Langmuir isotherm context. It is calculated using the Equation 4:

$$R_L = \frac{1}{1 + b\, C_0} \quad (4)$$

Where,

R_L = separation factor, b = Langmuir adsorption constant (L/mg) and C_0 = initial concentration of the adsorbate (ppm)

The Freundlich isotherm is an empirical model that describes adsorption on heterogeneous surfaces and assumes a multilayer adsorption process. Its equation is expressed as Equation 5 [33]:

$$\log q_e = \log K_f + \frac{1}{n} \log C_e \quad (5)$$

Where, q_e denotes the mass of adsorbate adsorbed per unit mass of adsorbent (mg/g). While C_e initial concentration of dye, the Freundlich constant is denoted by the symbol K_f (L/mg) and n represents the value of the empirical constant.

The adsorption mechanism is defined by the value of n: n = 1 indicating linear adsorption, n > 1 suggests chemisorption, and n < 1 corresponds to physisorption [34].

The Temkin isotherm considers the effects of indirect adsorbate–adsorbent interactions and assumes that the adsorption heat decreases linearly with surface coverage. Its equation is expressed as Equation 6 [33]:

$$q_e = \frac{RT}{b} \mathrm{Ln}\,(K_T . C_e) \quad (6)$$

Where, *b* is the coefficient of adsorption heat and K_T is the bonding equilibrium constant.

Kinetic analysis

To investigate the adsorption kinetics, both the pseudo-first-order (PFO) and pseudo-second-order (PSO) models proposed by Lagergren were applied. The PFO model is typically used to describe the initial stages of adsorption, whereas the PSO model is more suitable for chemisorption processes controlled by active site availability. These models are expressed in Equations 7 and 8, respectively [15,30]:

$$\mathrm{Ln}\,(q_e - q) = \mathrm{Ln}\, q_e - (K_1).T \quad (7)$$

$$\frac{t}{q} = \frac{1}{K_2 . qe^2} + \frac{t}{q_e} \quad (8)$$

Where, q_e (mg/g) is the amount of dye adsorbed at equilibrium, q (mg/g) is the amount adsorbed at time t, and k_1 and k_2 are the adsorption rate constants for the PFO and PSO models, respectively.

Thermodynamic studies

The effect of temperature on the adsorption process is commonly evaluated through key thermodynamic parameters, including the enthalpy change (ΔH°), entropy change (ΔS°), and Gibbs free energy change (ΔG°). These parameters provide insights into the spontaneity, feasibility, and degree of randomness associated with dye adsorption onto the adsorbent surface. When ΔH° is negative, the process releases heat (exothermic), while a positive ΔH° signifies heat absorption (endothermic). Reported ranges of ΔH° between –20 and 40 kJ/mol are typically

associated with physisorption, while values between –80 and –400 kJ/mol are indicative of chemisorption. A negative ΔG° value demonstrates that the adsorption is spontaneous, while a positive value signifies non-spontaneous behavior. Similarly, a positive ΔS° value suggests increased randomness at the solid–liquid interface, whereas a negative ΔS° value implies decreased randomness [35–37]. The values of ΔG°, ΔH°, and ΔS° were calculated according to the Equations 9-11:

$$\Delta G^0 = -R\,T\,Ln\,Kc \quad (9)$$

$$Kc = \frac{Cs}{Ce} \quad (10)$$

$$\Delta G^0 = \Delta H^0 - T\Delta S^0 \quad (11)$$

Where, R denotes the gas constant (8.314 J/mol. K), T is the temperature in K, and K_c is the equilibrium constant**.**

Results and Discussion

Characterization

The MOF-5 crystal structure was examined through XRD, as displayed in Figure 2a. The XRD pattern of MOF-5 is consistent with previously reported results [32,38]. The material exhibits characteristic diffraction peaks at 2θ values of 6.72°, 7.76°, 9°, 12°, 15°, 17.7°, 18.5°, and 19.7°, confirming its crystalline structure. The FTIR spectra of MOF-5 are presented in Figure 2b. A sharp absorption band at 1,573 cm^{-1} corresponds to the asymmetric stretching of the carboxylic group in the terephthalic acid linker. Several peaks in the region between 600 and 1,200 cm^{-1} are attributed to terephthalate-based vibrational modes. The region from 1,335 to 1,420 cm^{-1} is associated with asymmetric stretching vibrations of C–H bonds in the organic linker, whereas the bands at 2,947 and 3,438 cm^{-1} correspond to C–H and OH bending, respectively [39]. The SEM images of MOF-5 (Figure 2c) reveal irregular and fractured surface morphologies, which are characteristic of crystalline MOF structures. The fractured surfaces may be attributed to the intrinsic brittleness of MOF-5, while the irregular morphology suggests non-uniform crystal growth during the synthesis process. Such surface features are expected to increase the number of exposed active sites, thereby enhancing the adsorption capacity of the material [40,41].

The thermal stability of MOF-5 was evaluated using thermogravimetric analysis (TGA), as shown in Figure 2d. The TGA curve displays three distinct weight-loss stages, each corresponding to specific structural or compositional changes within the material. In the first stage, a 10% weight reduction observed below 150 °C is attributed to the removal of physically adsorbed water from the pores. The second major weight loss of about 47% between 200 and 400 °C corresponds to the onset of framework instability, where partial decomposition of the organic linkers occurs, reflecting the limited structural flexibility of MOF-5 at elevated temperatures. The final stage, extending up to approximately 800 °C, exhibits a total weight loss of 52.75%, which is associated with the complete collapse of the crystalline structure of MOF-5. These findings indicate that MOF-5 possesses good thermal stability up to nearly 400 °C, beyond which a pronounced structural degradation takes place [32,42].

The surface charge characteristics of the synthesized MOF-5 were evaluated by determining its point of zero charge (pHpzc). According to Figure 2e, the pHpzc was identified to be 6, indicating a neutral surface charge at this specific pH. In acidic environments (pH < 6), the MOF-5 surface acquires a positive charge. This proved advantageous for the adsorption of the anionic dye, as the attraction between the positively charged adsorbent molecules and the negatively charged dye molecules significantly accelerated the adsorption rate and increased the overall adsorption capacity [43].

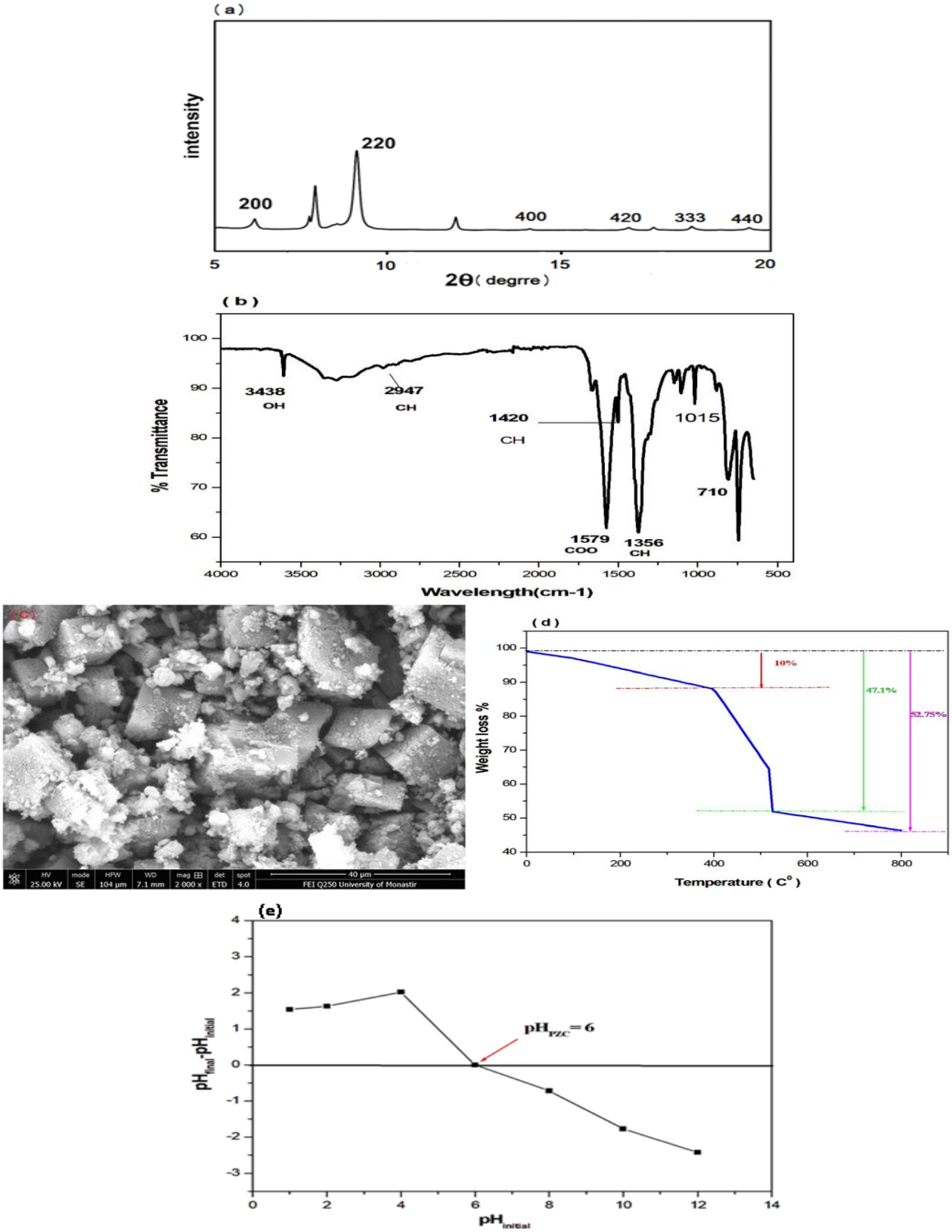

Figure 2. (a) XRD patterns, (b) FT-IR spectra, (c) SEM image, (d) TGA curve, and (e) pH_{PZC} of as- synthesized MOF-5

Adsorption experiments

Influence of pH

pH is a crucial factor in adsorption studies due to its significant influence on removal efficiency. In this study, all experiments were carried out at pH values ranging from 2 to 12, with a contact time of 2 hours, an initial TB dye concentration of 10 ppm, and a sorbent dose of 0.05 g/L at room temperature, as shown in Figure 3a. The results revealed that pH strongly affected TB removal efficiency, particularly under acidic conditions. The highest removal efficiency, approximately 59%, was achieved at pH 3. Comparable results have been observed for ZIF-67 and ZIF-67@ZnO composites, where maximum TB uptake was achieved at pH 5 [43]. This behavior can be attributed to the anionic nature of TB, as acidic conditions enhance adsorption by inducing a positively charged adsorbent surface, thereby strengthening electrostatic interactions. These observations are in good agreement with the findings of the present study [44,45], and all subsequent experiments were conducted at pH ~3.

Influence of doses

In adsorption processes, the adsorbent dosage plays a crucial role in determining the overall removal efficiency [16]. Therefore, selecting the optimal dosage is essential for effective TB dye removal. In this study, different concentrations of MOF-5 (0.01, 0.03, 0.05, 0.07, 0.1, 0.2, and 0.3 g/L) were investigated Figure 3b shows that the TB removal efficiency increased with increasing MOF-5 dosage, reaching a maximum of about 50% at the optimum dosage of 0.07 g/L. This improvement can be attributed to the higher number of available active sites on the adsorbent surface, which enhances dye–adsorbent interactions. However, at higher dosages, no further improvement was observed, possibly due to the saturation of dye binding sites and overlapping of adsorption layers, leading to reduced efficiency [43,45].

Influence of initial concentration

Determining the appropriate initial dye concentration is critical for achieving effective removal. In this study, the adsorption performance of MOF-5 was evaluated at TB dye concentrations ranging from 10 to 120 ppm, while other experimental parameters were kept constant. As shown in Figure 3c, the removal efficiency decreased from 77 to 41% with increasing dye concentration. This decline can be attributed to the limited number of active adsorption sites on MOF-5, which become saturated at higher dye concentrations, leading to surface accumulation and insufficient adsorption. Consequently, the optimum initial dye concentration for TB removal was determined to be 10 mg/L [46].

Influence of contact time

The interaction between the adsorbent and the dye molecules, and its influence on the overall adsorption process, can be evaluated by studying the effect of contact time. In this study, experiments were performed at different initial dye concentrations (10, 20, and 30 ppm) with contact times ranging from 10 to 240 min. Figure 3d shows a rapid increase in removal efficiency at the early stages across all concentrations. This rapid uptake indicates the abundance of available active sites on the MOF-5 surface, which facilitates strong adsorbate–adsorbent interactions. Over time, the adsorption rate gradually decreased, and equilibrium was reached at approximately 60 min, beyond which no significant increase in removal was observed. This behavior is attributed to the progressive occupation of active sites, reduced availability of vacant binding sites, and the establishment of a dynamic equilibrium between adsorption and desorption processes [47].

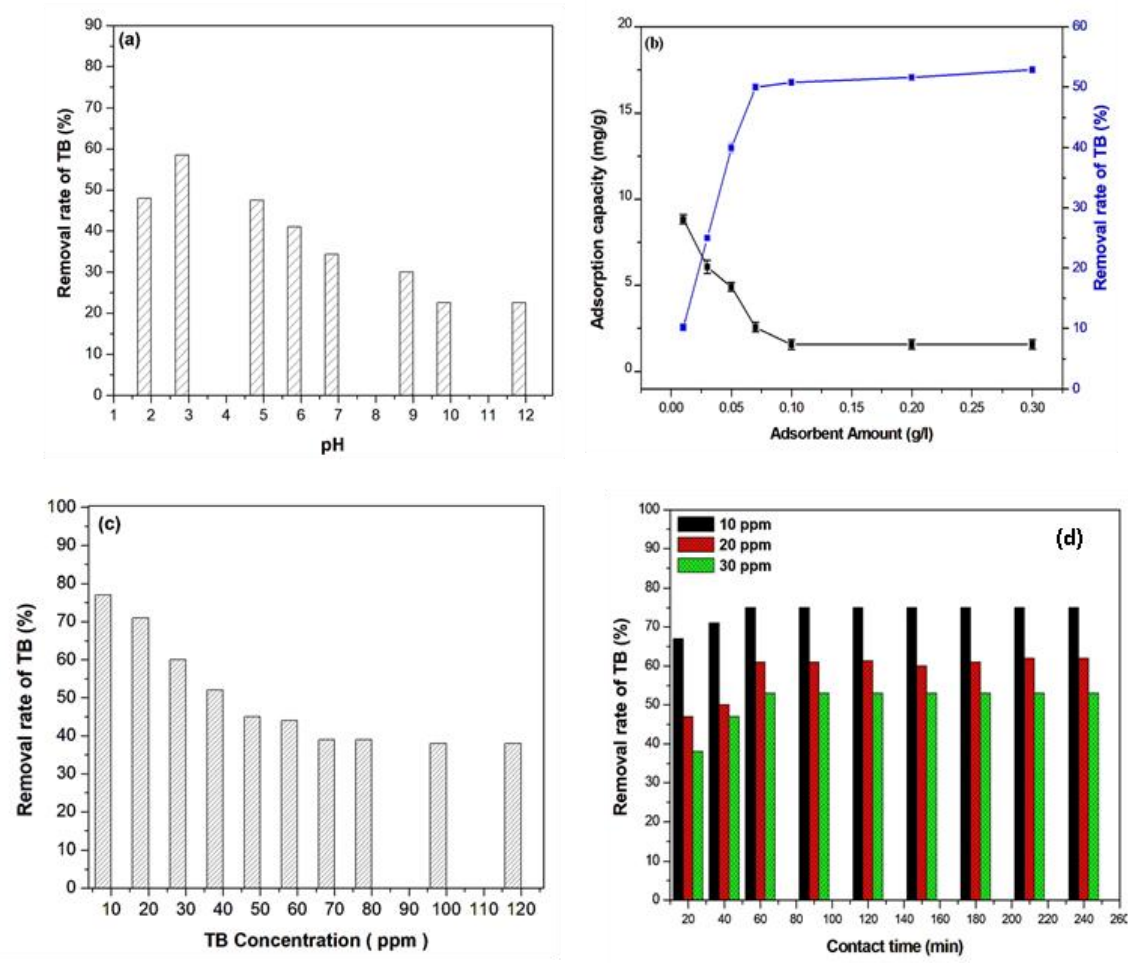

Figure 3. Batch adsorption experiments: (a) Influence of pH, (b) influence of adsorbent dose, (c) influence of initial concentration, and (d) influence of contact time at various initial dye concentration (10, 20. and 30 ppm)

Adsorption isotherms

The obtained data were analyzed using three isothermal models: Langmuir, Freundlich, and Temkin as shown in Figure 4. The results showed that all models exhibited good linearity. However, as presented in Table 1, a high correlation coefficient was obtained (R^2 = 0.999) for MOF-5 confirming the suitability of the Langmuir model, further supported by a separation factor (R_L) within the favorable range ($0<R_L<1$). These findings indicate that the adsorption process follows a monolayer adsorption mechanism, with a maximum adsorption capacity of 25 mg/g [43,48].

Adsorption kinetics

The PFO and PSO kinetic models were applied to investigate the adsorption process and extract its principal parameters. As shown in Figure 5, the correlation coefficients (R^2) obtained for the PSO model at all initial concentrations were higher than those of the PFO model. In addition, Table 2 indicates that the highest linear regression correlation coefficient (R^2) was achieved with the PSO model. Therefore, the PSO model demonstrated a superior ability to describe the adsorption of TB onto MOF-5 compared to the PFO model, suggesting that chemisorption governs the adsorption process of TB dye [49].

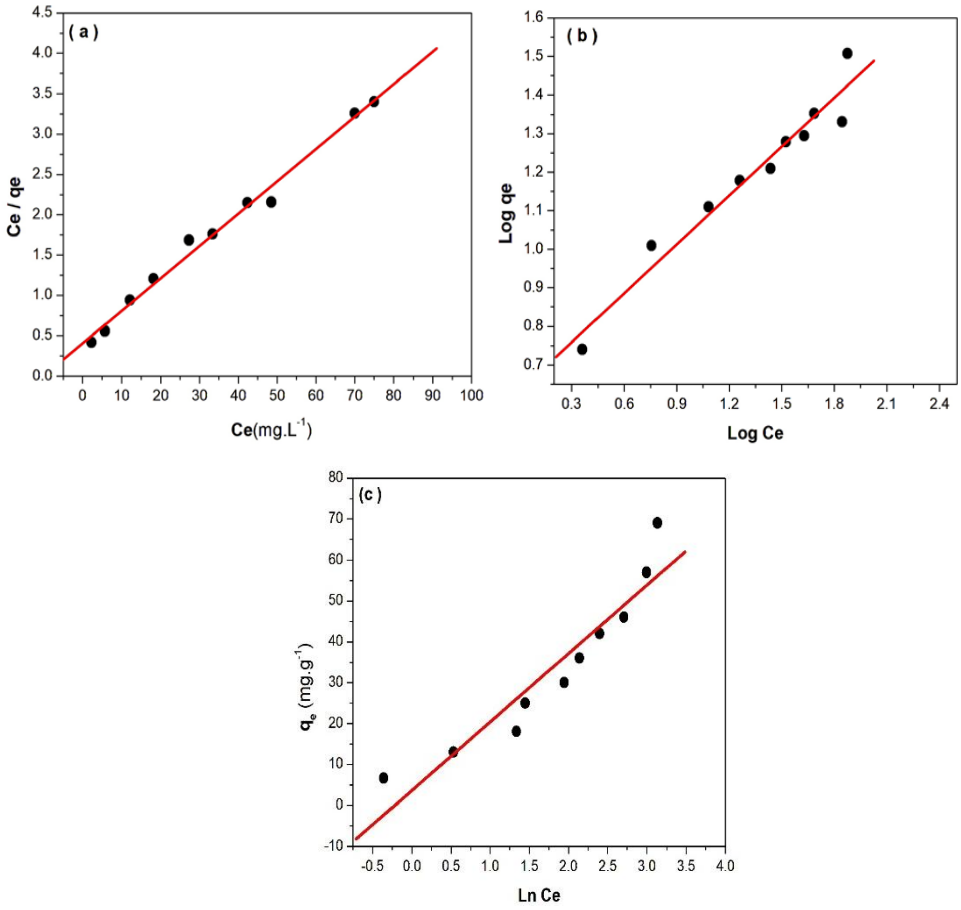

Figure 4. Adsorption isotherms of TB dye on MOF-5: (a) Langmuir isotherm, (b) Freundlich isotherm, and (c) Temkin isotherm

Table 1. Isotherm parameters for TB dye adsorption by MOF-5

Model	Parameters			
Langmuir	Q_{max}(mg/g)	B (mg/L)	R^2	R_L
	25	0.09	0.990	0.5
Freundlich	K_f	n	R^2	
	4.3	3.36	0.948	
Temkin	K_T(L/mg)	B_T (J/mol)	R^2	
	0.8	5.98	0.838	

Table 2. Kinetic parameters of TB adsorption onto MOF-5

Adsorbent MOF-5	Pseudo-first-order				Pseudo-second-order		
	C_0 (ppm)	qe (mg/g)	k_1 (min^{-1})	R^2	q_e (mg/g)	k_2 (min^{-1})	R^2
	10	1.22	-0.00008	0.236	5.4	0.089	0.999

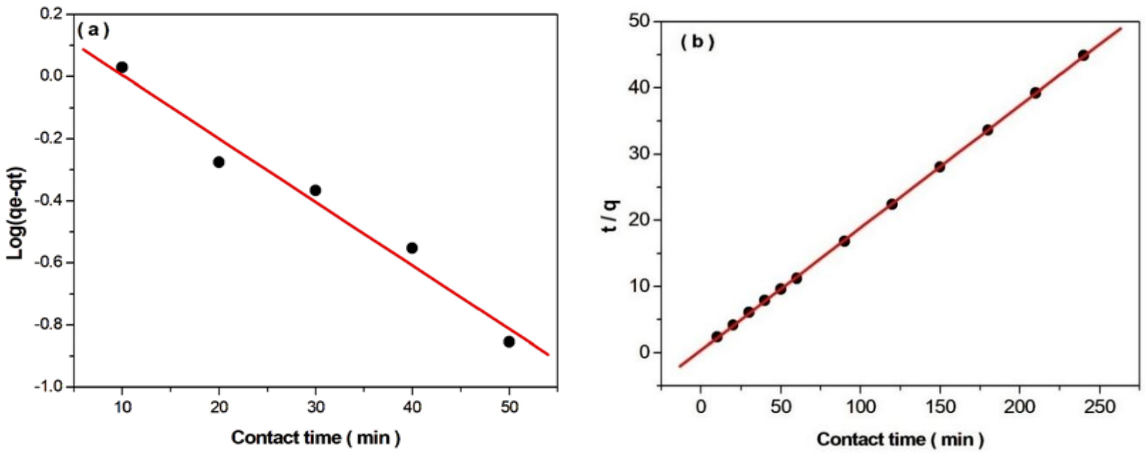

Figure 5. Kinetics analysis of MOF adsorption (a) pseudo- first- order model and (b) pseudo- second- order model

Table 3. Thermodynamic parameters of TB dye adsorption onto MOF-5

		ΔG° (KJ/mol)			
ΔH°(KJ/mol)	ΔS°(KJ/mol.K)	298.13	308.12	318.13	328.13
8.7	0.034	-1.4	-1.78	-2.11	-2.4

Adsorption thermodynamics

The thermodynamic parameters (ΔG°, ΔH°, and ΔS°) for the adsorption of TB dye onto MOF-5 are summarized in Table 3. The small negative ΔG° values (−1 to −2.4 kJ/mol) indicate that the adsorption process is feasible but driven by weak forces. This behavior is consistent with several previously reported studies on dye adsorption using MOF-based adsorbents, where ΔG° values typically fall within the range of −1 to −5 kJ/mol and are commonly attributed to physisorption governed by weak interactions such as van der Waals forces and electrostatic attractions, while the positive ΔH° and ΔS° values indicate its endothermic nature and the increase in disorder at the solid–liquid interface [50]. This behavior is now interpreted as a limited enhancement of adsorption with increasing temperature, possibly due to the increased mobility of dye molecules and improved accessibility of active sites [53].

Reusability test

The reusability of MOF-5 was systematically assessed to evaluate its practical applicability in repeated adsorption processes (Figure 6). The material underwent four successive adsorption–desorption cycles, during which the dye-loaded adsorbent was regenerated by washing with ethanol and subsequently dried prior to reuse. A marginal decline in the removal efficiency was observed even after the fourth cycle, demonstrating the remarkable structural integrity and recyclability of MOF-5. These results underscore its potential as a sustainable, robust, and economically viable adsorbent for wastewater treatment applications.

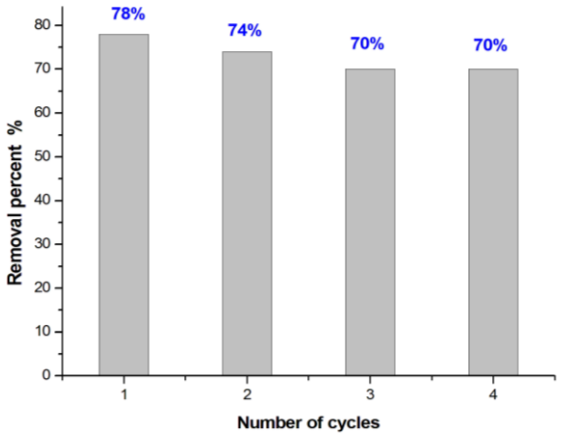

Figure 6. Cycling test of MOF-5

Table 4. A comparison of adsorption capacities of several adsorbents of TB dye

Adsorbent	pH	Temperature (K)	[TB] (ppm)	Dose (g/L)	Q_{max} (mg/g)	Ref.
MOF-5	3	298	10-120	0.07	25	The present study
Avocado seed powder	3	298	25	0.3	19.3	[16]
MgO	5.42	298	15-45	0.02	93.54	[15]
Fungal biomass	6	318	30-350	5	130	[16]
NZB LTH	4.5-5	298	5-30	0.08	5.3	[19]
Zn modified Luffa spong	7	303	10-50	1	47	[51]
PDDA/GO	6	298	0.001-1	0.01	50	[52]

Comparison of MOF-5 adsorption performance with other adsorbents

Compared with other adsorbents, the use of easily prepared and effective materials is essential for achieving satisfactory adsorption performance. In this context, MOF-5 stands out as it can be synthesized with relative ease while offering distinct structural and functional properties, making it a promising alternative to conventional adsorbents. Table 4 shows the adsorption capacity of MOF-5 at lower doses compared to other adsorbents. This superior performance at low adsorbent dosages highlights the high affinity of MOF-5 toward the dye molecules, which can be attributed to its high surface area, well-defined porous structure, and the availability of active adsorption sites, thereby enhancing its practical applicability in wastewater treatment [54].

Conclusion

The adsorption of the anionic dye TB onto MOF-5 synthesized via the solvothermal method was investigated. Characterization analyses confirmed that MOF-5 possesses suitable pore characteristics for adsorption. The adsorbent exhibited a relatively high adsorption capacity compared with other reported materials. Under optimized conditions (pH = 3, initial TB concentration = 10 ppm, and adsorbent dosage = 0.07 g/L), a removal efficiency of 77% was achieved within 60 min. Its strong agreement with the Langmuir model confirms that TB molecules were adsorbed in a uniform monolayer on the MOF-5 surface, with a maximum adsorption capacity of 25 mg/g. Thermodynamic and kinetic analyses revealed that the adsorption process is spontaneous and endothermic, and follows the pseudo-second-order kinetic model, suggesting a chemisorption mechanism. Moreover, MOF-5 maintained good performance after four cycles, supporting its potential for reuse. These results demonstrate that MOF-5 possesses a strong capability for dye removal and can serve as a practical, economical adsorbent for wastewater treatment. Therefore, scaling up the process from laboratory experiments to pilot- and industrial-scale applications could pave the way for its practical implementation in sustainable wastewater treatment systems.

Disclosure Statement

The authors declared that there were no conflicts of interest.

ORCID

Hajer Chemingui:
https://orcid.org/0000-0002-9095-8727
Hassan Aberrwaila:
https://orcid.org/0009-0008-0837-138X
Amor Hafiane:
https://orcid.org/0000-0002-1198-4354
Madiha Kamoun:
https://orcid.org/0000-0002-5989-3718

References

[1] Katheresan, V., Kansedo, J., Lau, S.Y. Efficiency of various recent wastewater dye removal methods: A review. *Journal of Environmental Chemical Engineering*, **2018**, 6(4), 4676–4697.
[2] Benkhaya, S., M'rabet, S., El Harfi, A. Classifications, properties, recent synthesis and applications of azo dyes. *Heliyon*, **2020**, 6(1), e03271.
[3] Chemingui, H., Rezma, S., Lafi, R., Alhalili, Z., Missaoui, T., Harbi, I., Smiri, M., Hafiane, A. Investigation of methylene blue adsorption from aqueous solution onto ZnO nanoparticles: Equilibrium and Box-behnken optimisation design. *International Journal of Environmental Analytical Chemistry*, **2023**, 103(12), 2716–2741.
[4] Beydaghdari, M., Saboor, F.H., Babapoor, A., Asgari, M. Recent progress in adsorptive removal of water pollutants by metal-organic frameworks. *ChemNanoMat*, **2022**, 8(2), e202100400.
[5] Djama, C., Bouguettoucha, A., Chebli, D., Amrane, A., Tahraoui, H., Zhang, J., Mouni, L. Experimental and theoretical study of methylene blue adsorption on a new raw material, cynara scolymus—A statistical physics assessment. *Sustainability*, **2023**, 15(13), 10364.
[6] Kenawy, E.-R., Ghfar, A.A., Wabaidur, S.M., Khan, M.A., Siddiqui, M.R., Alothman, Z.A., Alqadami, A.A., Hamid, M. Cetyltrimethylammonium bromide intercalated and branched polyhydroxystyrene functionalized montmorillonite clay to sequester cationic dyes. *Journal of Environmental Management*, **2018**, 219, 285–293.
[7] Beltrán, E.M., Pablos, M.V., Torija, C.F., Porcel, M.A., González-Doncel, M. Uptake of atenolol, carbamazepine and triclosan by crops irrigated with reclaimed water in a mediterranean scenario. *Ecotoxicology and Environmental Safety*, **2020**, 191, 110171.
[8] Adnan, M., Xiao, B., Ali, M.U., Xiao, P., Zhao, P., Wang, H., Bibi, S. Heavy metals pollution from smelting activities: A threat to soil and groundwater. *Ecotoxicology and Environmental Safety*, **2024**, 274, 116189.
[9] Cai, Z., Deng, X., Wang, Q., Lai, J., Xie, H., Chen, Y., Huang, B., Lin, G. Core-shell granular activated carbon and its adsorption of trypan blue. *Journal of Cleaner Production*, **2020**, 242, 118496.
[10] Kaur, H., Devi, N., Siwal, S.S., Alsanie, W.F., Thakur, M.K., Thakur, V.K. Metal–organic framework-based materials for wastewater treatment: Superior adsorbent materials for the removal of hazardous pollutants. *ACS Omega*, **2023**, 8(10), 9004–9030.
[11] Makhloufi, K., Samb, I., Srarfi, F. Clay-based ceramic membranes. *Advanced Ceramic Materials-Emerging Technologies*, **2024**, 3049- 8856.
[12] Mechi, L., Chemingui, H., Chékir, J., Alsukaibi, A.K., Azaza, H., Mhiri, M. Plant mediated green synthesis of zinc oxide nanoparticles for photocatalytic degradation of trypan blue: Optimisation via box-behnken design. *Results in Chemistry*, **2025**, 18, 102822.
[13] Hu, Q., Hao, L. Adsorption technologies in wastewater treatment processes. *Water*, **2025**, 17(15), 2335.
[14] Khedidja, M., Bechir, M., Feyda, S., Ali, T.M. Development of ceramic filtering membranes based on tunisian clay and phosphate sludge in wastewater treatment. *Solid State Sciences*, **2024**, 148, 107430.
[15] Priyadarshini, B., Patra, T., Sahoo, T.R. An efficient and comparative adsorption of congo red and trypan blue dyes on MgO nanoparticles: Kinetics, thermodynamics and isotherm studies. *Journal of Magnesium and Alloys*, **2021**, 9(2), 478–488.
[16] El-Idreesy, T.T., Khoshala, O., Firouzi, A., Elazab, H.A. Equilibrium and Kinetic Study on the Biosorption of Trypan Blue from Aqueous Solutions using Avocado Seed Powder. *Biointerface Research in Applied Chemistry*, **2021**, 11(3), 11042 – 11053
[17] Aracagök, Y.D. An investigation of the trypan blue dye's biosorption on fungal biomass. *Gümüshane Üniversitesi Fen Bilimleri Enstitüsü Dergisi*, **2023**, 13(3), 605-615.
[18] Chemingui, H., Missaoui, T., Mzali, J.C., Yildiz, T., Konyar, M., Smiri, M., Saidi, N., Hafiane, A., Yatmaz, H. Facile green synthesis of zinc oxide nanoparticles (ZnO NPs): Antibacterial and photocatalytic activities. *Materials Research Express*, **2019**, 6(10), 1050b1054.
[19] Sriram, G., Baby, N., Dhanabalan, K., Arunpandian, M., Selvakumar, K., Sadhasivam, T., Oh, T.H. Studies of various batch adsorption parameters for the removal of trypan blue using Ni-Zn-Bi-layered triple hydroxide and their isotherm, kinetics, and removal mechanism. *Inorganics*, **2024**, 12(11), 296.
[20] Andrew, F.P., Papo, T.R., Ajibade, P.A. Optimization of trypan blue and brilliant green dyes

photocatalytic degradation and adsorption of lead (II) and chromium (VI) heavy metal ions by copper sulfide nanoparticles. *Environmental Advances*, **2024**, 17, 100575.

[21] Zhu, R., Chen, Q., Zhou, Q., Xi, Y., Zhu, J., He, H. Adsorbents based on montmorillonite for contaminant removal from water: A review. *Applied Clay Science*, **2016**, 123, 239–258.

[22] Pouramini, Z., Mousavi, S.M., Babapoor, A., Hashemi, S.A., Lai, C.W., Mazaheri, Y., Chiang, W.-H. Effect of metal atom in zeolitic imidazolate frameworks (ZIF-8 & 67) for removal of dyes and antibiotics from wastewater: A review. *Catalysts*, **2023**, 13(1), 155.

[23] Soltani, Z., Hoseinzadeh, M., Saboor, F.H. Biomass gasification process enhancing using metal-organic frameworks. *Advanced Journal of Chemistry, Section A*, **2024**, 7(1), 89–109.

[24] Shams, P., Panahi, H., Tahan, M., Jahansooz, F., Heidaripour, A. Fabrication of curcumin (CCM) delivery system based on ZIF-8 nanoparticles (ZIF-8@ CCM) with anticancer application. *Journal of Medicinal and Nanomaterials Chemistry*, **2023**, 5(4), 267-275.

[25] Sajjadnejad, M., Haghshenas, S.M.S. Metal organic frameworks (MOFs) and their application as photocatalysts: Part II characterization and photocatalytic behavior. *Advanced Journal of Chemistry, Section A*, **2023**, 6(2), 172–187.

[26] Petit, C., Bandosz, T.J. Enhanced adsorption of ammonia on metal-organic framework/graphite oxide composites: Analysis of surface interactions. *Advanced Functional Materials*, **2010**, 20(1), 111–118.

[27] Mohammadi, A.A., Moghanlo, S., Kazemi, M.S., Nazari, S., Ghadiri, S.K., Saleh, H.N., Sillanpää, M. Comparative removal of hazardous cationic dyes by MOF-5 and modified graphene oxide. *Scientific Reports*, **2022**, 12(1), 15314.

[28] Mohammed, M.T.E., Djamel, N., Mohamed, T., Amokrane, S. Study of the adsorption of an organic pollutant onto a microporous metal organic framework. *Water Science and Technology*, **2021**, 83(1), 137–151.

[29] Kumar, G., Masram, D.T. Sustainable synthesis of MOF-5@ GO nanocomposites for efficient removal of rhodamine B from water. *ACS Omega*, **2021**, 6(14), 9587–9599.

[30] Saeed-Ul-Hassan, M., Ehtisham, M., Badawi, A.K., Khan, A.M., Khan, R.A., Ismail, B. A comparative study of moisture adsorption on GO, mof-5, and GO/MOF-5 composite for applications in atmospheric water harvesting. *Nanoscale Advances*, **2024**, 6(14), 3668–3679.

[31] Zhang, S., Ding, J., Tian, D., Su, W., Liu, F., Li, Q., Lu, M. Preparation of novel poly (sodium p-styrenesulfonate)/sodium alginate hydrogel incorporated with MOF-5 nanoparticles for the adsorption of Pb (II) and tetracycline. *Journal of Molecular Structure*, **2024**, 1300, 137313.

[32] Asadevi, H., Prasannakumaran Nair Chandrika Kumari, P., Padmavati Amma, R., Khadar, S.A., Charivumvasathu Sasi, S., Raghunandan, R. ZnO@ MOF-5 as a fluorescence "turn-off" sensor for ultrasensitive detection as well as probing of copper (II) ions. *ACS Omega*, **2022**, 7(15), 13031–13041.

[33] Chemingui, H., Riahi, R., Salem, W.B., Dbouba, H., Bensacia, N., Hannechi, A. Modified ceratonia siliqua as low-cost biosorbent for paracetamol removal: Equilibrium study and optimization via box-behnken design. *Biomass Conversion and Biorefinery*, **2025**, 15, 17887–17904.

[34] Chemingui, H., Lafi, R., Missaoui, T., Montasser, I., Hafiane, A., Kamoun, M. Eco-friendly approach for the synthesis of zinc oxide nanoparticles (ZnO NPs) using verbena officinalis l: Enhancement of photocatalytic activity under UV light and application of response surface methodology. *Biomass Conversion and Biorefinery*, **2025**, 15(3), 4281–4299.

[35] Saghir, S., Xiao, Z. Facile preparation of metal-organic frameworks-8 (ZIF-8) and its simultaneous adsorption of tetracycline (TC) and minocycline (MC) from aqueous solutions. *Materials Research Bulletin*, **2021**, 141, 111372.

[36] Siyal, A.A., Shamsuddin, R., Low, A., Hidayat, A. Adsorption kinetics, isotherms, and thermodynamics of removal of anionic surfactant from aqueous solution using fly ash. *Water, Air, & Soil Pollution*, **2020**, 231(10), 509.

[37] Talha, K., Wang, B., Liu, J.-H., Ullah, R., Feng, F., Yu, J., Chen, S., Li, J.-R. Effective adsorption of metronidazole antibiotic from water with a stable Zr (IV)-MOFs: Insights from DFT, kinetics and thermodynamics studies. *Journal of Environmental Chemical Engineering*, **2020**, 8(1), 103642.

[38] Kanmaz, N., Yardimci, B., Demircivi, P. In situ synthesis of MIL-125 on cinnamon stick and improved via carboxymethyl cellulose: A sustainable approach for super-high crystal violet adsorption. *Journal of Colloid and Interface Science*, **2025**, 678, 366–377.

[39] Gupta, H., Saini, I., Singh, V., Singh, V., Yarramaneni, S., Grover, P. Fast decomposition of organic contaminant in wastewater using Zn and Mn bimetallic metal organic frameworks. *Polyhedron*, **2024**, 261, 117116.

[40] Kumar, G., Masram, D.T. Sustainable synthesis of MOF-5@ GO nanocomposites for efficient removal of rhodamine b from water. *ACS Omega*, **2021**, 6(14), 9587–9599.

[41] Zhang, N., Li, H., Xu, Z., Yuan, R., Xu, Y., Cui, Y. Enhanced acetone sensing property of a sacrificial template based on cubic-like MOF-5 doped by Ni nanoparticles. *Nanomaterials*, **2020**, 10(2), 386.
[42] Harisankar, A., Preethi, P., Sreeja, T., Rejani, P., Murali, M., Raghunandan, R. Zinc oxide functionalized MOF-5 for the adsorptive removal of Pb (II) metal ions and photocatalytic degradation of methylene blue dye in aqueous medium. *Ionics*, **2024**, 30(4), 2313–2331.
[43] Aberrwaila, H., Chemingui, H., Hafiane, A., Kamoun, M. Comparative efficiency of ZIF-67 and ZIF-67@ ZnO nanocomposites for trypan blue adsorption: Preparation and RSM modeling. *Nano Select*, **2025**, e70083.
[44] Shiri, M., Hosseinzadeh, M., Shiri, S., Javanshir, S. Adsorbent based on MOF-5/cellulose aerogel composite for adsorption of organic dyes from wastewater. *Scientific Reports*, **2024**, 14(1), 15623.
[45] Edoamodu, C.E., Nwodo, U.U. Decolourization of synthetic dyes by laccase produced from bacillus sp. NU2. *Biotechnology & Biotechnological Equipment*, **2022**, 36(1), 95–106.
[46] Chemingui, H., Kahloul, M., El Abed, B., Ben Amor, T., Hafiane, A. Green synthesis of zinc oxide nanoparticles using albizia procera leaf extract: Degradation of methylene blue dye via advanced oxidation process and box–behnken design. *Clean Technologies and Environmental Policy*, **2024**, 26(10), 3273–3295.
[47] Amari, A., Alawameleh, H.S.K., Isam, M., Maktoof, M.A.J., Osman, H., Panneerselvam, B., Thomas, M. Thermodynamic investigation and study of kinetics and mass transfer mechanisms of oily wastewater adsorption on UIO-66–$MnFe_2O_4$ as a metal–organic framework (MOF). *Sustainability*, **2023**, 15(3), 2488.
[48] Nazir, M.A., Bashir, M.S., Jamshaid, M., Anum, A., Najam, T., Shahzad, K., Imran, M., Shah, S.S.A., ur Rehman, A. Synthesis of porous secondary metal-doped MOFs for removal of rhodamine B from water: Role of secondary metal on efficiency and kinetics. *Surfaces and Interfaces*, **2021**, 25, 101261.
[49] Zhong, X., Lu, Z., Liang, W., Hu, B. The magnetic covalent organic framework as a platform for high-performance extraction of Cr (VI) and bisphenol a from aqueous solution. *Journal Of Hazardous Materials*, **2020**, 393, 122353.
[50] Saghir, S., Xiao, Z. Facile preparation of metal-organic frameworks-8 (ZIF-8) and its simultaneous adsorption of tetracycline (TC) and minocycline (MC) from aqueous solutions. *Materials Research Bulletin*, **2021**, 141, 111372.
[51] Nadaroglu, H., Cicek, S., Gungor, A.A. Removing trypan blue dye using nano-Zn modified luffa sponge. *Spectrochimica Acta Part A: Molecular and Biomolecular Spectroscopy*, **2017**, 172, 2–8.
[52] Wang, X., Liu, Z., Ye, X., Hu, K., Zhong, H., Yu, J., Jin, M., Guo, Z. A facile one-step approach to functionalized graphene oxide-based hydrogels used as effective adsorbents toward anionic dyes. *Applied Surface Science*, **2014**, 308, 82–90.
[53] Li, H., Eddaoudi, M., O'Keeffe, M., Yaghi, O.M. Design and synthesis of an exceptionally stable and highly porous metal-organic framework. *Nature*, **1999**, 402(6759), 276–279.
[54] Aziz, M., Hassan, R., Saeed-Ul-Hassan, M., Ehtisham, M., Almatawa, M.S., Badawi, A.K., Ismail, B. Efficient water capture under low humidity using Ni-modified MOF-5: Scalable atmospheric water harvesting systems. *RSC Advances*, **2025**, 15(41), 34003–34015.

HOW TO CITE THIS ARTICLE

H. Chemingui, H. Aberrwaila, A. Hafiane, M. Kamoun. Enhanced Trypan Blue Removal from Wastewater Using Surface-Modified MOF-5 Adsorbents. *Adv. J. Chem. A*, 2026, 9(7), 1348-1362.

DOI: 10.48309/AJCA.2026.562486.1983
URL: https://www.ajchem-a.com/article_241029.html